

SCIAMACHY IN-FLIGHT INSTRUMENT PERFORMANCE

H. Bovensmann⁽¹⁾, B. Ahlers⁽³⁾, M. Buchwitz⁽¹⁾, J. Frerick⁽⁷⁾, M. Gottwald⁽⁴⁾, R. Hoogeveen⁽²⁾, J. Kaiser⁽¹⁾, Q. Kleipool⁽²⁾, E. Krieg⁽⁴⁾, G. Lichtenberg⁽²⁾, R. Mager⁽⁵⁾, J. Meyer⁽¹⁾, S. Noël⁽¹⁾, A. Schlesier⁽¹⁾, C. Sioris⁽⁷⁾, J. Skupin⁽¹⁾, Chr. v. Savigny⁽¹⁾, M. W. Wuttke⁽¹⁾, J. P. Burrows⁽¹⁾

⁽¹⁾University of Bremen, Institute of Environmental Physics/Remote Sensing, P.O. ox 330440, 28334 Bremen, Germany

⁽²⁾SRON, Space Research Organization Netherlands, Sorbonnelaan 2, 3584 CA Utrecht, The Netherlands

⁽³⁾TNO TPD Space, PO Box 155, 2600AD Delft, The Netherlands

⁽⁴⁾Remote Sensing Technology Institute, German Aerospace Center, Oberpfaffenhofen, 82234 Wessling, Germany

⁽⁵⁾Astrium GmbH, Earth Observation Navigation & Science Division, 88039 Friedrichshafen, Germany

⁽⁶⁾Smithsonian Astrophysical Observatory, SAO, Garden Street, Cambridge, MA 02138, USA

⁽⁷⁾ESA ESTE, Postbus 299, NL-2200 AG Noordwijk ZH, The Netherlands

ABSTRACT

On 1st of March 2002 ENVISAT with SCIAMACHY on-board was launched successfully in a sun-synchronous polar orbit. SCIAMACHY is a passive remote sensing instrument, which measures solar back scattered and reflected light from the atmosphere in nadir and limb viewing geometries during the majority of an orbit. In addition solar and lunar occultation measurements will be performed regularly. Measurements are made with moderate spectral resolution (0.2 – 1.5 nm) simultaneously in eight spectral channels covering the spectral region between 240 and 2380 nm. After a few weeks of out gassing SCIAMACHY was switched on successfully and a complex procedure starts to check out the instrument in orbit and tune it to the optimum in-flight performance. Solar and atmospheric spectra were already taken since the begin of April 2002. During SODAP and commissioning phase the instrument functional and optical performance was verified and instrument calibration activities were started. These activities revealed that SCIAMACHY is performing well and as expected from on-ground calibration, with only one exception: the water ice condensation in channels 7 and 8. Nevertheless for this problem countermeasures are identified. This paper summarizes the status of SCIAMACHY after 6 months in orbit, with a major focus on the optical and pointing performance.

1 Introduction

SCIAMACHY (SCanning Imaging Absorption spectroMeter for Atmospheric CHartographY) is a spectrometer [1, 2] designed to measure sunlight transmitted, reflected and scattered by the Earth's atmosphere or surface in the ultraviolet, visible and near infrared wavelength region (240 nm - 2380 nm) at moderate spectral resolution (0.2 nm - 1.5 nm, see Table 1). SCIAMACHY will measure the earthshine radiance in limb and nadir viewing geometries and solar or lunar light transmitted through the atmosphere observed in occultation. The extra-terrestrial solar irradiance and lunar radiance will be determined from observations of the sun and the moon above the atmosphere. The absorption, reflection and scattering behaviour of the atmosphere and the Earth's surface is determined from comparison of earthshine radiance and solar irradiance. Inversion of the ratio of earthshine radiance and solar irradiance yields information about the amounts and distribution of important atmospheric constituents and the spectral reflectance (or albedo) of the Earth's surface. SCIAMACHY was conceived to improve our knowledge and understanding of a variety of issues of importance for the chemistry and physics of the Earth's atmosphere (troposphere, stratosphere and mesosphere) and potential changes resulting from either increasing anthropogenic activity or the variability of natural phenomena.

Inversion of the SCIAMACHY measurements enables the amounts and distribution of the atmospheric constituents O₃, O₂, O₂(¹Δ), O₄, BrO, OCIO, ClO, SO₂, H₂CO, NO, NO₂, NO₃, CO, CO₂, CH₄, H₂O, N₂O, and aerosol, as well as knowledge about the parameters pressure p, temperature T, radiation field, cloud cover, cloud top height and surface spectral reflectance to be determined. A special feature of SCIAMACHY is the combined limb-nadir measurement mode. The inversion of the combination of limb and nadir measurements will enable tropospheric column amounts of O₃, NO₂, BrO, CO, CH₄, H₂O, N₂O, SO₂ and H₂CO to be determined.

The SCIAMACHY instrument is a passive remote sensing moderate resolution imaging spectrometer. It comprises a mirror system, a telescope, a spectrometer, and thermal and electronic sub systems. The incoming radiation enters the instrument via one of three ports:

- (i) for nadir measurements the radiation from the Earth's scene is directed by the elevation mirror into a telescope (off axis parabolic mirror) which focuses the beam onto the entrance slit of the spectrometer,
- (ii) for limb and solar/lunar occultation measurements the radiation is reflected by the azimuth mirror to the elevation mirror and then into the telescope which focuses the beam onto the entrance slit of the spectrometer,
- (iii) for internal and sub-solar calibration measurements the radiation of internal calibration light sources or the solar radiation is directed by the elevation mirror into the telescope.

Except the scan mirrors, all spectrometer parts are fixed and the spectra are recorded simultaneously from 240 nm to 1750 nm, and in two smaller windows, 1940 nm - 2040 nm and 2265 nm - 2380nm, in the near infrared. The spectral and radiometric performance of the SCIAMACHY spectrometer is summarized in Table 1.

	Channel	Spectral Range [nm]	Resolution [nm]	Stability over orbit [nm]
High Resolution Channels	1	240 - 314	0.24	0.003
	2	309 - 405	0.26	0.003
	3	394 - 620	0.44	0.004
	4	604 - 805	0.48	0.005
	5	785 -1050	0.54	0.005
	6	1000 -1750	1.48	0.015
	7	1940 - 2040	0.22	0.003
	8	2265 -2380	0.26	0.003
Polarization Measurement Devices	PMD1	309 - 377	Broadband	
	PMD2	450 – 522	Broadband	
	PMD3	610 – 701	Broadband	
	PMD4	806 – 908	Broadband	
	PMD5	1505 – 1642	Broadband	
	PMD6	2297 – 2392	Broadband	
	PMD 7 (45°)	805 – 908	Broadband	
Radiometric Accuracy		2 -4 %		

Table 1. SCIAMACHY Optical Performance Parameters. Note: data in channel 1 will available down to 220 nm with reduced calibration accuracy.

The SCIAMACHY instrument performance was verified on-ground and an extensive calibration program was performed within the development of SCIAMACHY [3]. The on-ground calibration program has been carried out in a special thermal vacuum facility (OPTEC) with which a flight representative environment was established, i.e. vacuum and with the temperature distribution in the SCIAMACHY instrument adjusted to values expected for the in-flight situation. The calibration program yielded a set of key parameters, representing a sound quantification of the instrument performance characteristics. The key parameters have been used for implementation in the level 0 to 1b processor.

While the stabilised temperature distribution in the instrument, achieved after opening of the radiant cooler door and the optical ports of the instrument, is found to be very close to the temperatures maintained in the ground calibration program, the key parameters are also applied in the analyses addressed in this first performance assessment. From these initial - and forthcoming results of the performance analyses, which are still on going, reasons to update one or more ground calibration key parameters may be identified. An example of an already identified necessity to update a key parameter is the bad/dead pixel table for infrared detectors. This and any other change in keydata will then be processed and implemented in the SCIAMACHY data processing algorithms accordingly.

One focus of the activities during SODAP and Cal/Val is the verification of the instrument performance in-flight in the areas of spectral, radiometric and pointing performance as well as the identification of any unexpected behaviour in-flight. The first results are summarised in the following chapters.

2 Spectral Performance

2.1 Spectral calibration

The on ground spectral calibration was performed with internal and external calibration sources. The spectral calibration polynomial coefficients are derived from the on-ground spectral calibration of SCIAMACHY [4] are based on spectral line source (SLS) measurements for channels 1 to 6 and on tracegas absorption spectra for channels 7 and 8 [5]. These polynomial fits are used as the precise basis of the spectral calibration of the level 1 data (SPECTRAL_BASE in level 1b products). The current implemented spectral calibration for channel 8 is only valid for the lower 200 pixels of this channel. For the upper part of channel 8 this results in a wavelength shift of the spectral calibrated (ir)radiances. This on-ground calibration has to be verified, monitored and updated in-flight. On an operational level this is done with the internal line source (SLS) and optionally by the analysis of Fraunhofer lines. Till now only internal SLS spectra have been analysed. During SODAP a preliminary spectral calibration analysis of the internal SLS spectra was performed. 106 out of the 108 spectral lines defined in the keydata could be fitted. The fitted line positions agree with the positions predicted in the keydata within ± 0.5 pixel which is as good as it can be because the predicted positions are given as integers i.e. without a fractional part.

Fig. 1 shows the difference between the in-flight spectral calibration derived from this 106 lines and the on-ground spectral calibration. The difference is in the range of ± 0.05 nm for channels 1 to 6. Using the internal SLS as only calibration source for channel 7 and 8 has some known drawbacks: There are only 2 SLS lines in channel 7 which are used to derive shifts for the on-ground spectral calibration. In channel 8 there are 5 lines but all of them are located in the upper half of the channel which leads to a deviation of up to 0.3 nm in the long wavelength part of channel 8. Spectral calibration in channels 7 and 8 has to be improved by using spectral information from atmospheric absorptions, similar to the approach already applied for the on-ground spectral calibration.

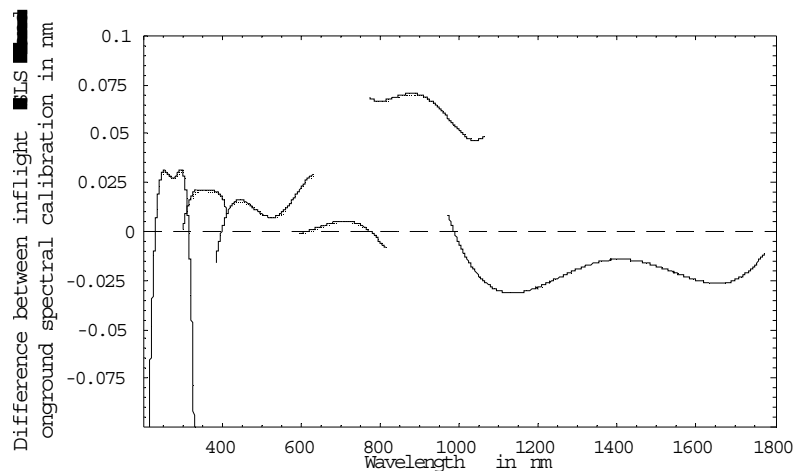


Fig. 1. Difference between the in-flight spectral calibration and the on-ground spectral calibration.

The orbit stability of the spectral calibration is close or less a 1/100 pixel, in-line with the requirements. The SLS line positions is currently also very stable over month as the in-flight spectral calibrations derived from SLS spectra from orbits 906 to 2500 vary only within ± 0.02 nm.

2.2 In-flight verification of the slit function

The detailed knowledge about the slit function is relevant for accurate convolution of the spectra (cross-section, atmospheric etc.) used within the level 1-2 retrieval step. Fig. 2 demonstrates that there is on average no significant change in the slit function between on-ground and in-flight configuration. Nevertheless single lines show variations of up to 0.1 pixel, which is probably a result of the slight spectral undersampling of measurements.

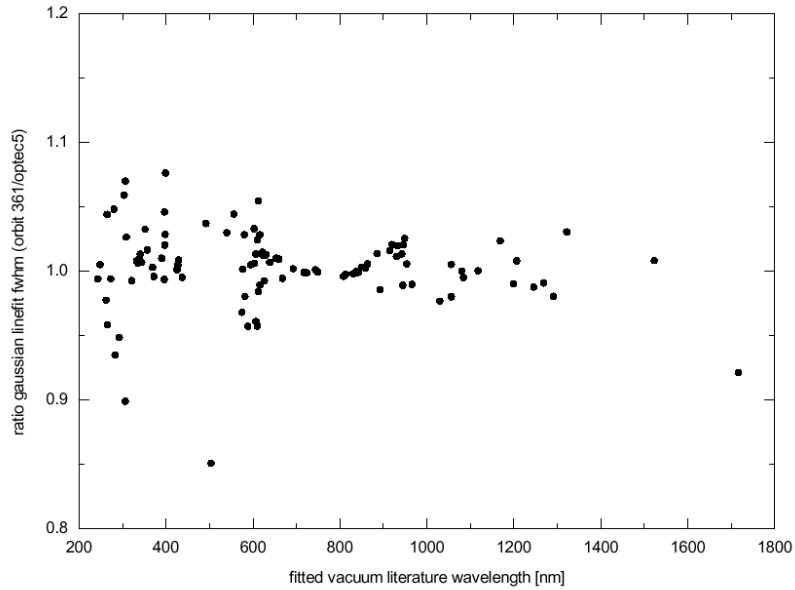


Fig. 2. Ratio of calculated Gaussian FWHM from fitted literature vacuum wavelength between Orbit 361 and OPTEC 5 (both internal SLS).

During on-ground calibration the difference in the slit function between internal and external calibration was characterised [6] and it was found that the slit function determined by the internal SLS is approx. 0.1 pixel (depending on the channel) smaller than that determined with an external SLS, due to a partial blocking of the light path of the internal SLS. This behaviour is confirmed for the in-flight configuration as can be seen for channel 1 in Fig. 3. Fig. 3 shows the time series of the mean slit function in channel 1 (internal SLS, derived by a Gaussian fit) compared with the mean Gaussian slit function given in the keydata (external SLS). The slit function is quite stable over time. Similar is observed for channels 2 to 6. For channels 7 and 8 it is very difficult to determine accurately the slit function due to the higher noise level and fewer spectral lines. In the near future the slit function has to be investigated by using atmospheric and solar spectra.

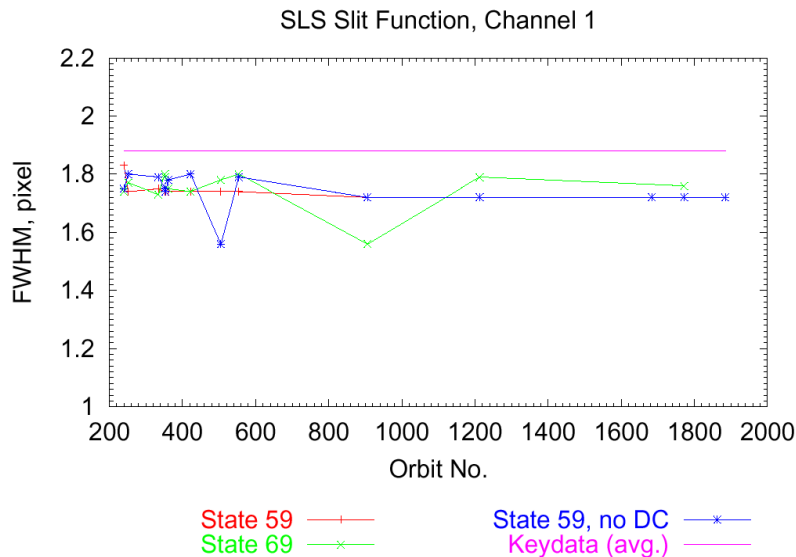


Fig. 3. Time series of the mean slit function in channel 1, retrieved with the measurements of the internal SLS, compared with the mean slit function given in the keydata, which are retrieved with the external SLS measurements.

2.3 Tangent height dependent spectral shift

Besides the methods mentioned in sections 2.1 and 2.2 a spectral calibration can also be derived with shift and squeeze algorithms that fit the in-flight measured atmospheric radiances to known tracegas absorption spectra. First results of that method for limb measurements showed a tangent height dependent wavelength shift of the measured radiances. In Fig. 4 (left) the spectral shift derived by the fitting algorithms is presented. It is in the range of 0.005 nm in the BrO fitting window and 0.015 nm in the NO₂ fitting window.

Doppler shift and the influence of the slope of the spectrum on the retrieved line positions [7] can be excluded as origin of this effect because they are one order of magnitude too small. In [8] it is concluded that the inhomogeneous illumination along the short dimension of the instrument slit (dispersion direction, elevation in limb) caused by the strong tangent height dependent gradient of the earth shine radiances in limb geometry explains the observation in a quantitative way. The modelled results of this effect is shown in Fig. 4 (right) and is up to 0.008nm (~ 0.08pix). They are in good agreement with the spectral shift observed in the measured spectra. A detailed report on this topic is available [8].

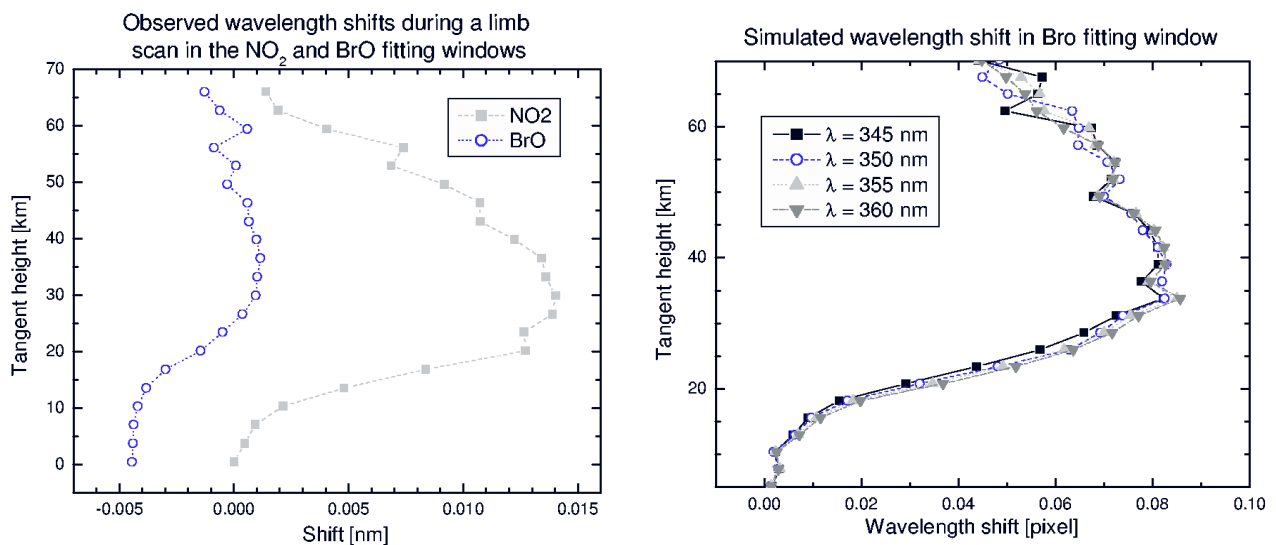


Fig. 4. Observed (left) and modelled (right) tangent height dependent spectral shift derived from limb radiances. (0.1nm ~ 1pix, Orbit 797, limb state 7, date: 04/25/2002, geog. lat.: 56-59N, geog. long.: 238-253, 18:30 UTC)

Retrieval algorithms performing shift-and-squeeze fit on the spectral axis will be less effected by the tangent height dependent spectral shift. It has to be noted that also the slit function itself might be affected by the inhomogeneous illumination of the spectrometer slit in dispersion direction. A tangent height dependent spectral shift is also found in occultation geometry [9].

3 Radiometric Performance

3.1 Instrument Throughput / Etalon

In this section we deal with two different aspects. The first aspect is the overall throughput of the instrument. This can be tested with the White Light Source (WLS). For a reliable monitoring it is necessary to first compare the performance of the WLS in-flight with the performance on-ground. The second aspect is the stability of spectral features caused by the so-called etalon effect that was already observed in GOME.

3.1.1 WLS comparison on-ground vs. in-flight

The purpose of the WLS is to correct pixel-to-pixel gain, check the overall throughput of the instrument and correct for changes in the etalon effect (see below), if any.

In the first in-flight measurements taken with the WLS it became obvious that the signal was higher than expected. At the same time the output of the spectral line source (SLS) was as expected. This pointed to a change of the WLS as the reason for the higher output, since the SLS and the WLS share the same optical path. Further investigations identified a temperature increase of the lamp filament of around 100 K as the cause for the different behaviour in-flight and on-ground (see Fig. 5).

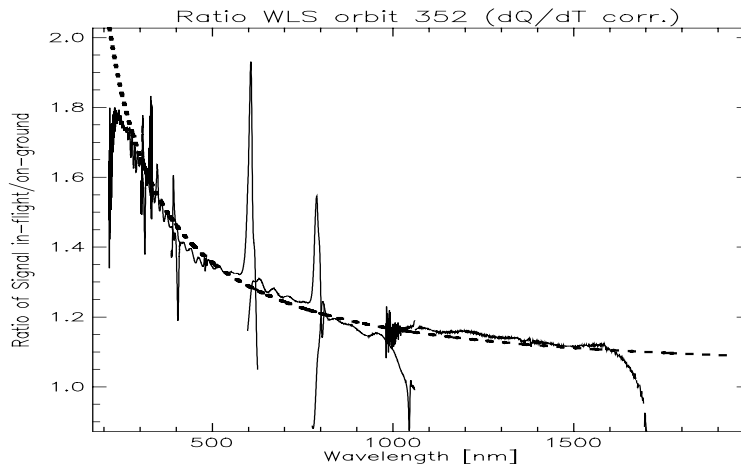


Fig. 5. Ratio between WLS measurement on-ground and in-flight. The dashed line shows the ratio between a Planck curve calculated with the on-ground lamp temperature and a 95 K higher temperature. The high values at the channel boundaries come from the division of values near zero.

The higher temperature is probably caused by microgravity leading to a lower convection within the lamp. This causes a higher temperature of the lamp filament. However, the lamp output has been stable so far, thus no serious consequences for the calibration of the instrument because of the higher lamp output is foreseen.

3.1.2 Transmission in channels 1 to 6

After correcting the in-flight WLS measurements for the enhanced filament temperature (see Fig. 5), the ratio of the internal WLS to the on-ground reference WLS measurement gives an early indication about changes in the instrument throughput between on ground and in-flight. Fig. 6 gives an example from orbit 635, where only the limb port was open (SRC door and nadir door closed). The overall changes in the instrument throughput are at least within 2.5% and are dominated by etalon like structures, expected deviations in the overlap regions and not completely corrected temperature dependence of the quantum efficiency due to the special thermal conditions in that orbit. Note that a degradation in the UV (below pixel 1000) is not observed at that point in time, but later during commissioning phase (see below).

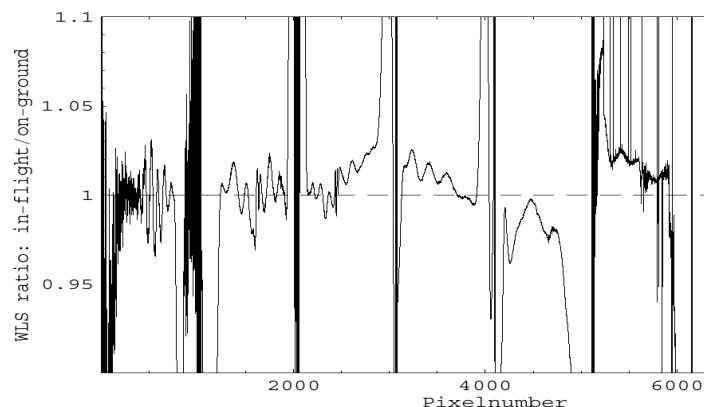


Fig. 6. Transmission of channels 1-6 as determined from WLS measurements on-ground and in-flight (Orbit 635) and including a correction for the enhanced WLS temperature in-flight.

3.1.3 Transmission in channel 7 and 8

After the cool down of the detectors to nominal temperatures a constant loss of transmission in channels 7 and 8 was observed. The reason for the decreasing transmission is a slow build-up of ice on the detectors of these channels. The other channels show no transmission loss due to ice. Fig. 7 below shows the development of the transmission from begin of July to end of August. The first peak is a nominal decontamination where the detectors are heated to up to 240 K. The second peak is caused by the special decontamination where in addition to a heating of the detectors to 270 K the OBM was heated to 260 K. After the decontaminations the detectors return to their nominal temperature. The data are normalised to the transmission at 170 K, where it is certain that there is no ice on the detectors. One can clearly see that after the special decontamination the transmission decrease is slower than after the nominal decontamination. There are three possible reasons for that:

- An accumulated effect of both decontaminations
- The special decontamination was more effective in removing the water from the direct surroundings of the detectors, but the total water content in the instrument is the same. This would lead to a slower decrease of transmission but to the same final level of transmission as for nominal decontaminations
- The special decontamination actually reduced the total amount of water in the instrument

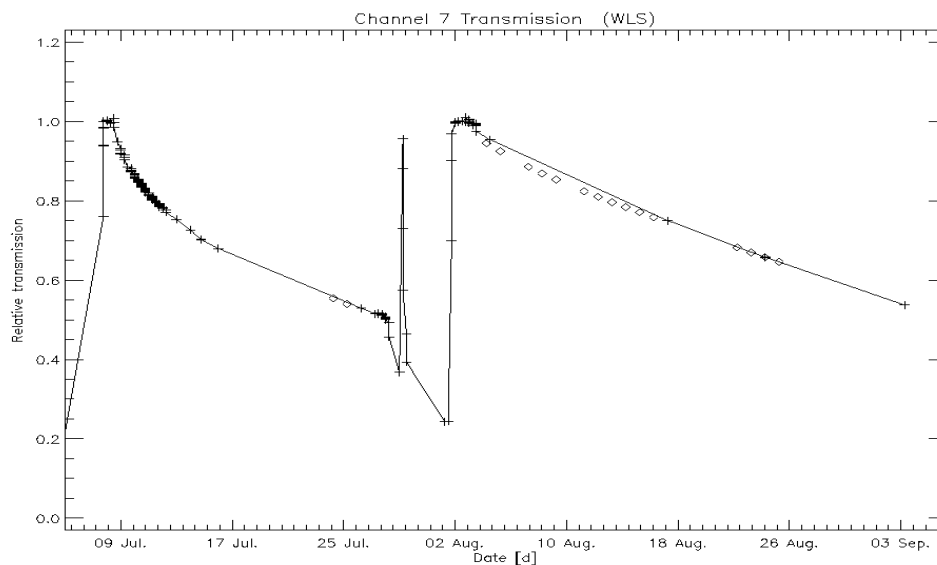


Fig. 7. Development of transmission after nominal decontamination (first peak) and special decontamination (second peak). Shown is the average intensity in the channel 7. The diamonds are ESM diffuser measurements scaled to the WLS measurements.

A clear conclusion can only be made after more data are available. At the moment there are efforts under way to avoid the ice build-up altogether by changing part the operational concept. Although the loss of transmission is serious, even with reduced transmission it is already possible to retrieve reasonable column amounts of trace gases absorbing in channels 7 and 8 [10,11].

3.1.4 Etalon effect in channels 1-5

The so-called etalon effect is already known from GOME. It is visible in the spectra as a periodic oscillation, with a period getting longer with wavelength. The effect is caused by multiple reflections between the light detecting Si layer of the Reticon detectors and their protective SiO₂ layer. The effect as such poses no problem for the data quality since it is characterised on-ground. However, a very thin ice layer of a few nanometer leads to a phase shift of the etalon induced oscillation.

If the ice layer is changing in time, oscillations will appear in the calibrated spectra and can diminish the quality of the derived data products (as was observed in GOME). Model calculations using data from a special measurement campaign during the commissioning phase give – depending on the channel – maximum ice layers of 0.4 to 2 nm assuming all observed oscillations are caused by ice (see Fig. 8).

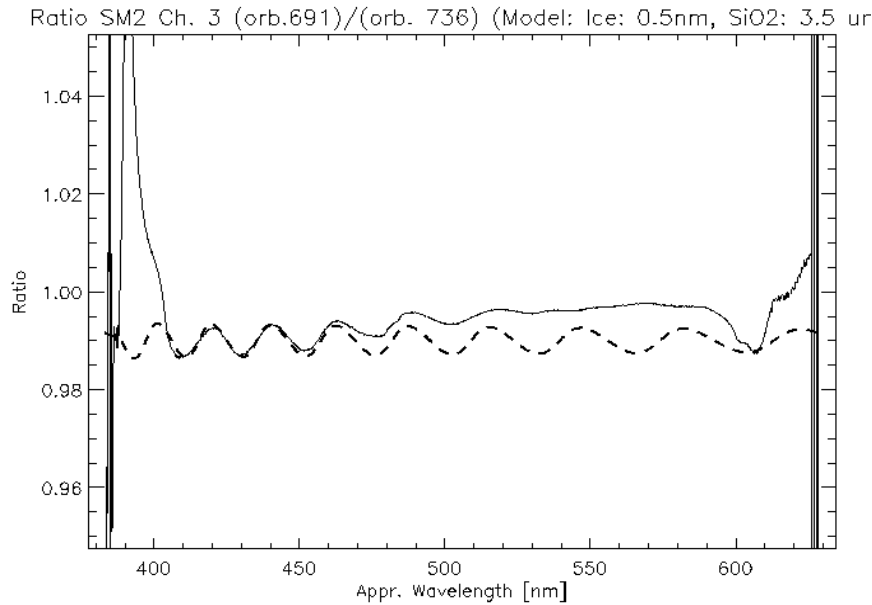


Fig. 8. Ratio of a WLS measurement at high detector temperature (= free of ice) to a measurement at low temperatures in channel 3 (solid line). The dashed line represents the model calculation (4 nm ice layer).

A water molecule has a diameter of around 0.32 nm. The maximum variation the calculated ice layer would induce in the spectra is around 1% which is an order of magnitude lower than observed in GOME. However, it seems more likely that the observed changes are caused by slight thermal shifts of the optical bench and/or the detectors, which could also lead to small phase shifts mimicking the effect of an ice layer. A more important test is the stability of the oscillation. A comparison of data taken 47 days apart showed no change in the oscillation. Thus we can conclude that the transmission in channels 1 to 5 is free of changing etalon induced structures and there is no ice build-up in these channels. The stability of the detector etalon is a major improvement in comparison to the strong variations in the detector etalon as observed by GOME.

3.2 Detector Dark Signal.

3.2.1 Introduction.

Even when the SCIAMACHY instrument is not exposed to light, the detectors will still have a certain output. This output is known as the detector dark signal. This dark signal of the SCIAMACHY science detectors has four distinct contributions:

- A time independent contribution added by the electronics referred to as the analogue offset or the fixed pattern noise (FPN). The term FPN is an inheritance from the original data sheets by RETICON; this term is misleading and therefore the term analogue offset will be used throughout this document.
- A time dependent contribution caused by thermally created electron-hole pairs. This contribution is the true leakage current and depends on the bias voltage applied, as well as the temperature of the detector material.
- A time dependent contribution due to spatial stray light.
- A time dependent contribution from the thermal background radiation. This can only be noticed in the infrared detection range, viz. channel 6+, 7 and 8.

The thermal background is present in all measurements, and scales linearly with the pixel exposure time (PET). Hence, it can not be distinguished from the true leakage current and is therefore included implicitly in the dark current.

For all purposes this poses no problem because it constitutes a stable contribution as long as the optical bench module (OBM) is stable in temperature.

The contribution due to spatial stray light also scales linearly with the pixel exposure time, but is not necessarily stable in time. It has been shown that spatial stray light is present in all dark current measurements in the sunlit part of the orbit. In addition, the first records in each state suffer from pick up of spurious signal at state initialisation. This is most likely due to atmospheric light entering the slit when the scan mirrors move from their idle position into the

measurement position. Exclusion of the first records proved not to be sufficient due to a prolonged memory effect. It was shown that the memory effect sustained much longer than earlier anticipated something that is due to the fact that the determination of the dark current requires accuracies of sub-binary level. The classic memory effect has only been characterised up-to several readouts because it was assumed it was of no importance below 1 binary unit. Therefore, measurements taken in the sunlit part of the orbit can not be used for the determination of the detector dark current and are excluded from all result presented in this document.

The contribution from the thermal background depends only on the temperature of the optical bench module. The emission is assumed to be broadband and diffuse, and not to contain any spectral features.

3.2.2 In-flight determined leakage current.

The leakage current can be determined by taking two measurements of the detector output with different pixel exposure times. Per pixel, a straight line can be fitted through the two points; the intersection at the y-axis at PET $t=0$ s now gives the analogue offset, while the slope yields the leakage current in binary units per second.

Albeit those two points are sufficient to determine a straight line, three points with different exposure times are used, allowing for a more accurate determination of the fitting parameters if a least squares algorithm is used. For this purpose three dark current states were implemented, having state id's 46, 63 and 67. During the SODAP phase, different versions of these states have been tested, and the optimised states will be used during nominal operations. The complete description of the algorithm is documented in [12] and [13].

In Table 2, the mean value of the leakage current is calculated by taking the average over all pixels in each channel; channel 6+ is listed separately from channel 6. The error specified is the 1 sigma error as returned by the least squares algorithm. The temperature given in the table is the actual detector temperature averaged over the eclipse. The factor is the conversion factor per channel, which is used to transform from BU to amperes. The last two columns give the leakage current and temperature as measured during DM tests [14]. The leakage currents indicated with an * in column 7 are in [fA /mV]; because they scale linearly with the applied bias voltage.

Channel	LC	Error LC	LC	T detector	factor	LC	T detector
	In-flight					On-ground	
	[fA]	[fA]	[BU/s]	[Kelvin]	[e/BU]	[fA]	[Kelvin]
ch1	0.00244	0.03104	0.0311	204.40	490	0.009	200
ch2	0.00567	0.03544	0.0414	203.85	855	0.011	200
ch3	0.05763	0.03794	0.4212	223.10	854	0.049	220
ch4	0.05472	0.04328	0.3935	221.64	868	0.061	220
ch5	0.04796	0.04297	0.3469	219.79	863	0.17	230
ch6	0.01252	0.04906	0.1477	198.62	529	0.005*	200
ch6+	5.82139	0.11725	68.6842	198.62	529	14*	200
ch7	12.16050	0.24770	428.8095	148.23	177	5-12*	150
ch8	100.92262	0.25405	3558.7820	146.95	177	10-50*	150

Table 2. Leakage current (LC) averaged over all pixels in each channel for orbit 2085.

The results in Table 2 lead to the following conclusion:

- Channel 1 and 2: The leakage current in channel 1 and 2 is in line with data measured during the DM test, if one takes into account the error bars; however, the in-flight derived measurements seem to be considerably lower and better. Because the in-flight measurements reproduce very well over many orbits we believe that these are correct. The leakage current in this channel is extremely low at 0.0025 fA or 0.031 BU/s; it takes approximately 30 seconds pixel exposure time before the leakage current is above the 1 BU measurement threshold. Furthermore, the error in the derivation of the analogue offset is approximately 1 BU, which therefore introduces a much larger error. Taking into account the maximum integration time for any scientific measurement state during nominal operation (state NAD01: 10s; state LIMB01: 1.5s), we propose to ignore the leakage current correction for this channel.
- Channel 3 to 5: The leakage current in channel 3 to 5 is completely in line with the DM test, especially when corrected for differences in detector temperatures. For the longest limb state, the contribution of the leakage current to the measurement amounts to 4 binary units; with an 0.7 BU error from the analogue offset correction. For this channel the correction for the leakage current can only be omitted if other calibration errors are much larger than this value.

- Channel 6 to 8: Channel 6 to 8 are operated a zero bias voltage, which means that it theoretically has no leakage current. The in-flight measured values, as well as those from the DM test are very low and consistent with each other within the specified error bounds. The error in the estimation of the analogue offset in these channels is 4 binary units at maximum, while the array-averaged dark signal can reach 3700 BU/s in channel 8. Accurate correction is of paramount importance.

In order to derive the temperature coefficients for the leakage current in the RETICON detectors, we have taken all leakage current and temperature data per channel and plotted $\log(I)$ versus $(1/T)$. In Fig. 9, the results are given for channel 5; also shown is the fitted straight line whose slope corresponds to $(-E_{\text{gap}}/k)$.

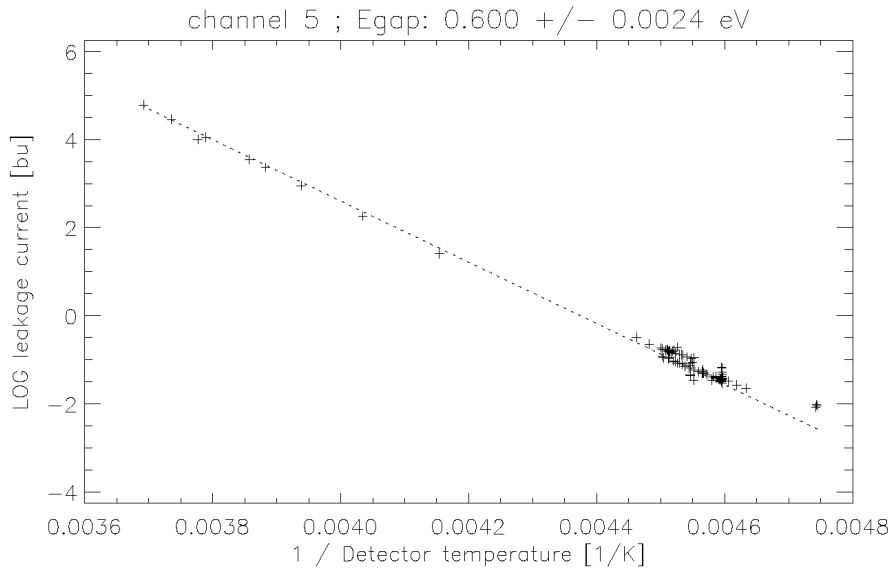


Fig. 9. Temperature dependency of the leakage current for channel 5, derived from in flight data.

The dependency of the leakage current with temperature in channels 1 to 5 is governed by Boltzmann's Law, and hence can be modelled accurately. Using these derived values the leakage current at different temperatures can be calculated to high precision. Details about first results on temperature dependence of the leakage current are documented in [15]

3.2.3 Conclusion

The main conclusion is that detectors have not changed since the last detector module (DM) test, neither can changes be measured between the pre-flight and in-flight detector performance. All the detectors have analogue offsets and leakage currents as expected from the DM test. The leakage currents can be well characterised in the eclipse of each orbit. There is no indication for the presence of spatial stray light in this orbit phase. The leakage currents for channels 1 to 5 are even lower than those measured during the DM test. Especially for channel 1 and 2, the leakage current is very low; they even could be omitted in the calibration algorithm for the level 0 to level 1 data processor. For these channels the correction for the analogue offset suffices, the random error made in this is approximately 1 binary unit, which is much less than the leakage current correction. Channel 6-8 dark signal is dominated by the thermal background. The contribution of the true leakage current is negligible because these detectors are operated at nearly zero bias voltage. The in-flight data shows that the actual operation bias voltage is indeed close to zero. In addition the temperature dependence of the leakage current in channels 1-5 can accurately calculated.

4 Degradation Monitoring

4.1 Introduction

Monitoring the behaviour of SCIAMACHY in-orbit is an essential function during the Commissioning and Routine Operations Phase. It ensures that

1. the actual instrument status is known
2. countermeasures preventing instrument malfunctions can be initiated
3. data processing can incorporate the most up-to-date instrument characterisation

Here we will mainly stress the last point as it is the most crucial and most urgent task of monitoring which affects immediately all users of SCIAMACHY data. The whole concept of monitoring the instrument is described in [16].

Fig. 10 depicts the basic interfaces of the so called Operational Long Term Monitoring (OLTM), for which the SCIAMACHY Operations Support Team (SOST) is the responsible entity. The Monitoring function ingests all kind of data products up to level 1b and the housekeeping data, produces reports on the instrument state and even feeds back information into the data processing chain. The latter is of major concern as the mission reaches the end of the commissioning phase with the ground segment being not in a satisfactory state concerning data distribution and quality of the data products.

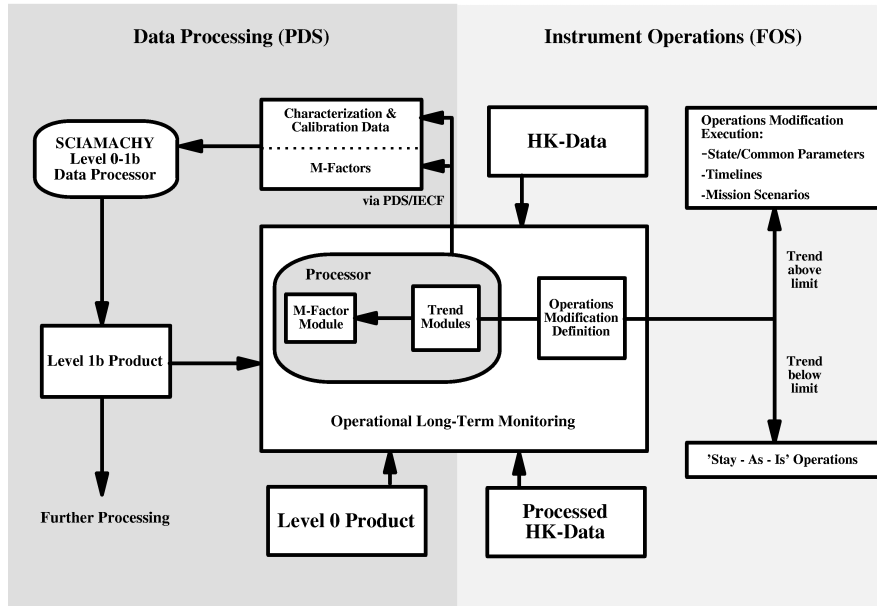


Fig. 10. Functional interaction of the Operational Long Term Monitoring with PDS and FOS

4.2 The M-factor concept

In theory we describe the incoming light by a Stokes vector, and the path of the light through the instrument to the detectors as a product of Müller matrices, one for each component. The detector signal then is just the first component of the resulting Stokes vector. The Müller matrix components are computed from the key data retrieved during the on-ground characterization of the instrument. We assume that degradation (i. e. deviation from the on-ground characterization) then can be described as a scalar factor on each Müller matrix. Thus we have a set of so called aging coefficients for each component that can be distinguished by such a model, namely α for the ASM, ϵ for the ESM, δ for the Diffuser, ω for the optical bench module to the science detectors, ν for the NDF, γ for the optical bench module to the PMD's 1-6, and ρ for the optical bench module to PMD 7.

If monitoring would indicate a non-scalar matrix-like degradation this would result in a recommendation to change the key-data. At the beginning of the mission when the instrument is assumed to be well characterized by the key-data, all aging coefficients are defined as being equal to 1.

M-factors are used in the 0-1b processor to compensate for this radiometric degradation of SCIAMACHY. In general, a m-factor is defined as a product of inverse aging coefficients and can be determined as the ratio between a measured solar spectrum at the time t to a reference spectrum obtained for the same optical path at the time 0, i.e. BOL. Ideally, these reference spectra should be taken on-ground, but in practice this is not possible because measurements of the unobscured sun cannot be performed on-ground. Therefore, "earliest" in-flight measurements shall be taken as reference. It is assumed that the instrument didn't change significantly between the key-data measurements and the

Thus for each optical path an m-factor has to be computed that will compensate the degradation of the components in this path, namely m_{cal} for the calibration light path (via diffuser, NDF) to the science detectors, m_{dl} for the limb light

path to the science detectors, m_{pl} for the limb light path to the PMD detectors 1-6, m_{ql} for the limb light path to the 45° PMD detector, m_{dn} for the nadir light path to the science detectors, m_{pn} for the nadir light path to the PMD detectors 1-6, and m_{qn} for the nadir light path to the 45° PMD detector.

Naturally each m-factor is defined to be equal to one at a time where the instrument is well characterized by the actual set of key-data. A consistent set of m-factors is computed on timescales derived from the trends that SOST identifies in the instrument behaviour. This set of m-factors is delivered to the IECF and applied to all data that are calibrated in the Level 0 to 1b processing.

The strategy of the m-factor concept is as follows: The m-factors shall be computed on the basis of calibrated sun spectra, where the calibration shall be consistent with the operational L0-1b processing. The latter point is very crucial as one has to carefully avoid to apply corrections twice. Exactly those corrections that the Level 0-1b processor applies have also to be applied to those spectra that are used to compute the m-factors. Therefore tools are derived from Level 0-1b processor prototype software package. Currently the progress in implementing the m-factor concept is limited by the availability of the up to date version of the L0-1b processor prototype software package and the unavailability of a consistent set of consolidated level 1b data for the past month.

4.3 Results from level 0 products

Due to the lack of sufficient level 1b data at the moment, monitoring activities have to utilize the level 0 products. Based on the analysis of level 0 data the instrument seems to show signs of degradation, as can be seen from Fig. 11 where ratios of WLS spectra are plotted against pixel number. In Fig. 11 these spectra are taken from orbit 1684 and orbit 2401, 2 months apart. A similar behaviour is observed for orbit 906 and orbit 1684, also 2 months apart. Besides the well known effect of ice in channels 7 and 8 we already see a substantial loss of transmission in the UV channels 1 and 2. The assumption m-factor = 1 is therefore already obsolete and an extrapolation to zero degradation has to be included. One can suspect that the cause of this transmission loss is degradation of the involved ESM mirror. Such a degradation has been observed in GOME [17]. For the ASM at least the aging coefficient α can be determined without a reference spectrum. This would give a first hint about the deviation from the assumption $m_{ql} = 1/\alpha \epsilon \omega = 1$.

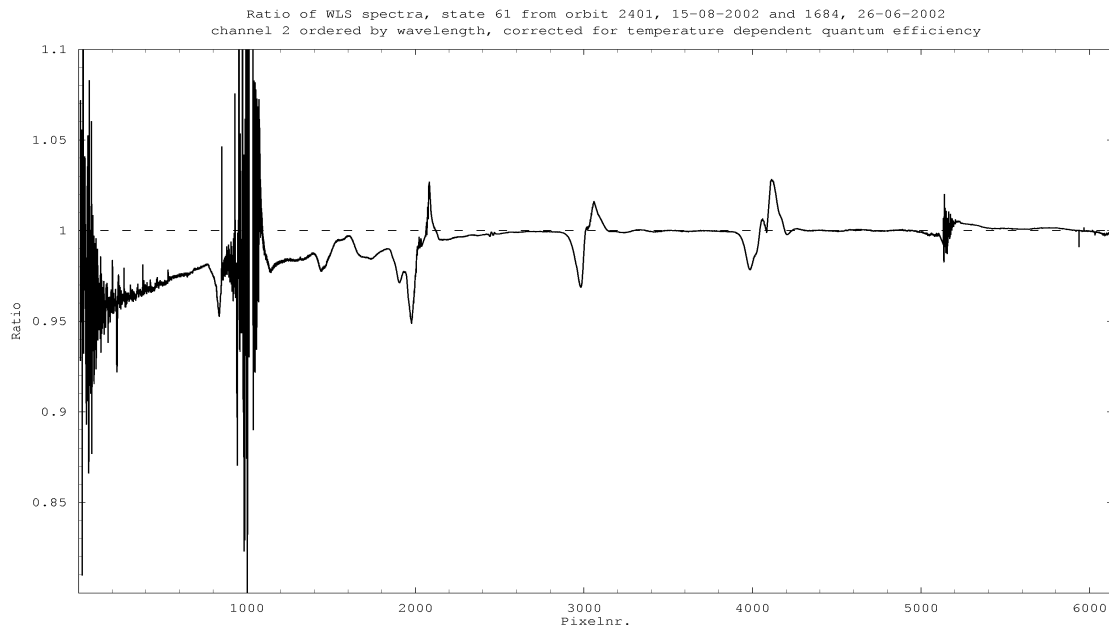


Fig. 11. Ratio of internal WLS measurements indicating a degradation in the UV

4.4 Conclusions

The monitoring function is strongly related to the in-flight calibration function and contributes directly to the quality of the data products. Preliminary monitoring in the commissioning phase shows that the instrument is altering already, as expected from the experience with GOME. The basic idea of the m-factor concept, that the instrument didn't change between on ground characterization (key-data) and early in-flight phase, is thus waning. The Operational Long Term

Monitoring concept depends on the level 1b product. To fulfil the task of monitoring a reliable distribution of a sound consolidated level 1b product together with the up to date version of the L0-1 processor prototype package is outstanding.

5 SCIAMACHY pointing performance via Sun Follower System (SFS)

5.1 Introduction

SCIAMACHY Pointing capabilities have been verified during the first part of the SODAP by executing specially designed measurement states and the nominal Sun and Moon states:

- Sun occultation measurements in the atmosphere
- Sun calibration measurements above the atmosphere
- Sun calibration measurements via sub-solar calibration window (slit)
- moon occultation measurements in the atmosphere
- moon calibration measurements above the atmosphere

The special states performed were developed to derive the centring of the Instantaneous Field of View (IFoV) of SCIAMACHY on the celestial target used.

5.2 Observation Modes used by SCIAMACHY SFS-states

The SCIAMACHY observation modes for the above measurements are

- Nominal scan (saw-tooth)
- Fast-sweep (trapezoid motion generating signal integration by a fast linear motion across the celestial target)
- Tracking the target using pre-calculated and commanded target position and angular rate data (one or two axis)
- Pointing to the target centre by one or both of the scan mirrors using
- Sub-solar observation implies the usage of the elevation scan mechanism (ESM) only

The execution of the measurement state is the final step of a long chain of preparatory/planning co-operation with Astrium starting with the definition of the goal of the measurement by the scientific community respectively the engineering team in charge for a particular performance aspect and ending with the transmission of the commands for pre-calculated target position and rate and execution timing parameters to SCIAMACHY. SODAP operations planning and execution is described in [18].

5.3 Usage of the SFS for state execution

The SFS is used for the acquisition and tracking of the celestial target. This can be performed independently in two axis for the azimuth scan mechanism (ASM) and the elevation scan mechanism (ESM). In all scientific measurements designed for nominal SCIAMACHY operations every scanning motion over the Sun or the moon is implemented for the ESM due to the vertical structure of the atmospheric phenomena investigated. Thus the centring of the IfoV in azimuth direction during the scan execution is an important requirement to be fulfilled by the SFS, in particular for all sun target measurements, where the IfoV is reduced by an aperture stop to 0.7° in azimuth. The control system for the steering of the scan mechanisms is operated for these pointing tasks either in 'closed loop' with the SFS active or in 'open loop' with the SFS inactive. In closed loop the scanners are controlled such that an image of the target is kept centred on the calibrated 'middle' of the SFS, which is a quadrant cell of FoV $2.1^\circ \times 2.1^\circ$ (during sun observations also reduced in azimuth to 0.7°). In open loop the control system can follow the sun track by acquiring the commanded initial target position and following the target track with given angular rates. This mode is also used for calibration measurements using diffusers attached to the back of the scan mirrors.

5.4 Selected examples of scan execution data

5.4.1 Sun observation nominal scan - short duration

The scientific requirement for this state is, that the Sun is observed when ascending through the atmosphere, whereby a scan in elevation direction shall be performed. To fulfil this requirement, state and associated timeline are designed such, that the Sun is picked up when the solar disk appears at the horizon. Due to refraction in the atmosphere, which

has to be accounted for twice for spaceborne observations of celestial targets, the line of sight (LoS) from the instantaneous position of SCIAMACHY to the Sun is diverted such, that the Sun appears at the geometric height of the Earth horizon, when it is geometrically still about 60km below it. Furthermore the apparent shape of the Sun is at that moment distorted to a flat disk, which develops to the nominal circular disk during the initial phase of the ascent. To overcome anticipated problems with acquiring the Sun already in the low atmosphere in the first part of the state, the ESM-scan motion is centred at a geometric height of 17.2km and the ASM is moved to the pre-calculated position of the Sun-rise. Based on model calculations the Sun is acquired 32 seconds after start of the measurement with the ASM by the SFS when it has reached about 40 km height. From then on the Sun is actively tracked while the ESM continues its scan motion following the predicted sun track. Fig. 12 displays the ESM (left) and ASM (right) position against time.

Fig. 12 (left) shows that while waiting in scanning mode for the Sun to appear no signal is recorded by the PMD and that during ascent the elevation dimension of the Sun increases. In the upper part of the atmosphere the signal level remains constant. This fact is obvious in the final phase of the state in a height of approx. 100 km where the ESM stopped the scan motion and is pointing to the Sun centre and the PMD signal is static. The yellow circles mark the Sun centre as derived from the signal and the violet dots over the ESM position visualise the positions, where the PMD signal indicates, that the SCIAMACHY IFoV was directed to within the Sun disk. It can be seen, that the elevation scan is not perfectly centred over the Sun but still covers the full disk. The red line represents the extrapolated ESM position corresponding to the predicted elevation angle to which the scan motion is added.

Fig. 12 (right) shows also the position of the ASM scanner against time. The mirror start at the commanded position of the Sun and follows with the specified rate up to BCPS 512 (= 32sec). At that point in time acquisition of the Sun by the SFS is enabled resulting in a sudden 'small' jump in azimuth of 0.045° . In this diagram the circles representing the solar centroid are smaller scaled to show the slight asymmetry w.r.t. time of the passes through the Sun centre. The asymmetric sequence of the Sun centroid time stamps indicates again, that the ESM scan is not exactly centred on the Sun. The change in position is obvious, the reason for it is still not exactly known but one explanation could be again the effect of refraction in azimuth. Investigation is ongoing.

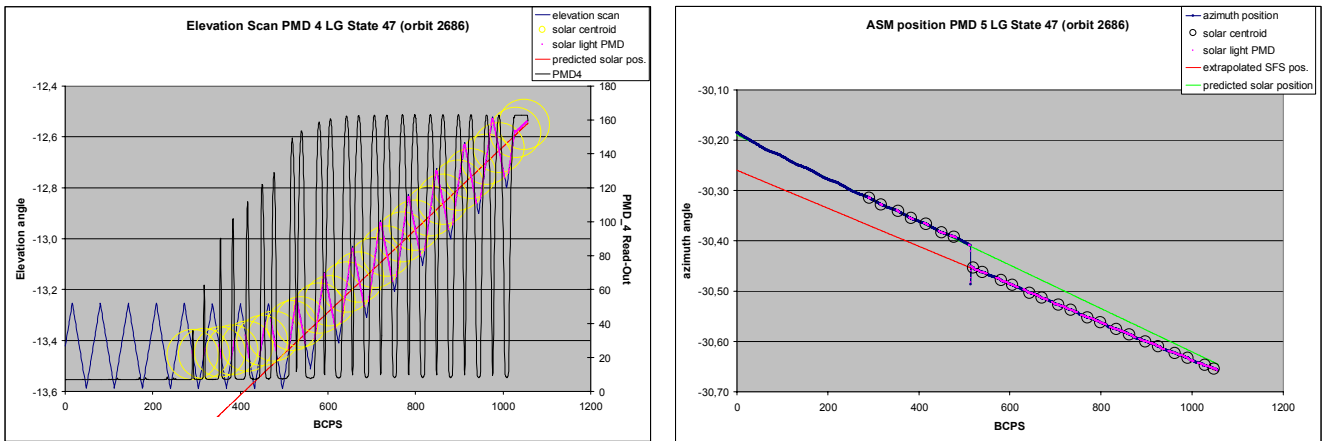


Fig. 12. ESM-scan and PMD_4 signal during sun occultation (left) and ASM-scan during sun occultation (right).

5.4.2 Sun observation fast sweep scan - sub-solar observation

This example displays the execution of a state in sub-solar observation condition i.e. when the Sun passes through SCIAMACHY's sub-solar slit window (= Nadir Calibration Window Mechanism - NCWM) corresponding to a position with mean Sun azimuth of 270° . Because of the slit dimensions the image of the full sun disk resides in the sub-solar window for only approx. 3.2 sec. Thus the timing of the start of the measurement has to be carefully designed. This is done in the execution of the state and as well in the observation conditions provided with the related timeline to the mission planning system (MPS), which calculates the parameters for the timeline start and the target acquisition respectively the alignment of SCIAMACHY LoS. The present implementation provides an angular peak-to-peak swing of 4.05° LoS. Within the signal integration time commanded of 125msec this angular motion results in an effective integration time of the Sun radiation of ca. 23 msec. The slope of the scan extreme positions is very small because of the sub-solar condition, as the Sun shows for this SCIAMACHY observation geometry nearly no motion in elevation. For nearly all scans two points for readings are visible. This is not in contradiction to the above statement of an

integration time of 125msec. For the evaluation of the scanner control the faster readouts of the PMD's are used, which produce data with a fixed frequency of 40Hz (see Fig. 13).

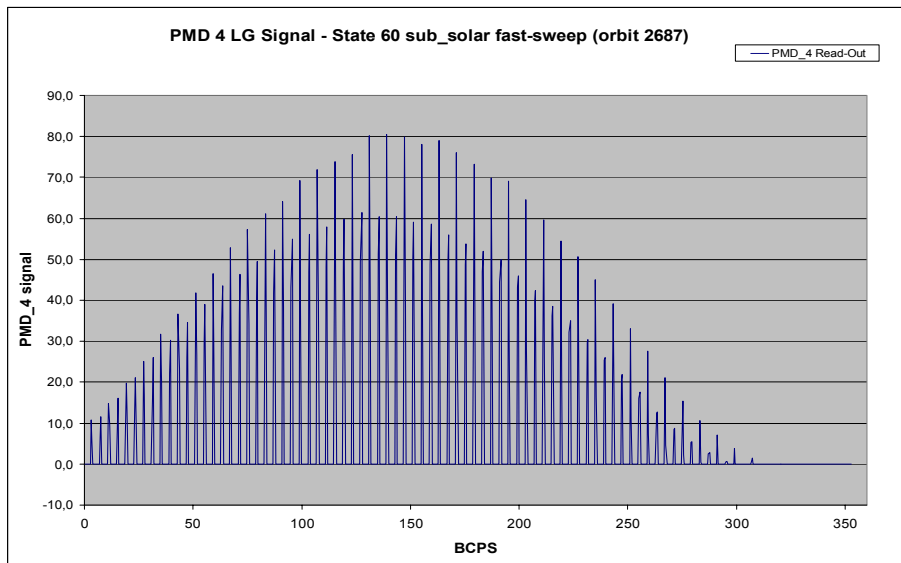


Fig. 13. ESM-scan sub-solar 'fast-sweep'

Fig. 13 shows the PMD4-signal measured during the state execution. The signal is slightly asymmetric in time, which is caused by a incorrect start time of the measurement. A modification of the timing conditions contained in the timeline file will correct this in the future.

5.4.3 Moon observation special ASM scan above atmosphere

This example illustrates the results of a special state designed for the verification of the SFS performance for moon observations. Here a scan motion in the azimuth direction is implemented. Due to the size of the FoV in azimuth of 1.82° and the apparent viewing angle of the Moon of 0.5° a scan motion of at least 2.3° peak-to-peak is required to yield data points where the moon is outside the FoV. Since the measurement is performed above the atmosphere the maximum values of all scans should be identical and have the same value as when pointing to the Moon centroid.

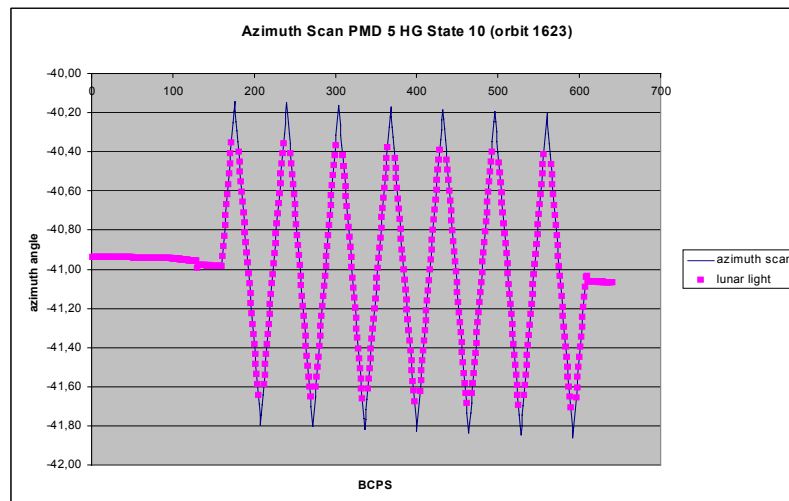


Fig. 14. ASM-scan Moon with pointing phases scanner read outs (left), PMD 5 data (right)

In the initial phase of the state the moon track is followed by using the predicted track parameters commanded. At 130 BCPS and 600 BCPS the SFS is commanded to acquire the moon centroid. Both signal values are the reference for the centre of the moon during the ASM scan motion. Fig. 14 shows the range, where moon light is observed and as well the centring at 130 and 600 BCPS. Between these 2 points the ASM executes a scan of 3.3° peak-to-peak LoS. The motion

of the target through the instrument FoV in azimuth can be seen from the slope of the extreme values and the difference of the positions at both acquisitions. The signal shift at initial acquisition of the moon is caused by the fact, that ASM and ESM acquire at that point the moon.

5.5 Performance values of the SFS

5.5.1 SUN target

During SODAP some features of the Sun and moon states had to be modified to correct for effects mostly to be attributed to disturbances of the SFS by atmospheric conditions.

- At low altitudes the SFS signal was regularly reduced to below the detection level by the extinction in the atmosphere. This caused error messages "loss of target" by the onboard computer. Changing the timing strategy for low Sun altitude (17km) cured this problem.
- Atmospheric effects caused also a jitter of the ESM in lower altitude pointing phases. After introduction of a delay for the time of the SFS actuation no more error entries were recorded.

The evaluation of the special and the nominal Sun states resulted in the following performance figures:

- Tracking of the Sun via prediction was performed within the specifications applicable for the nominal scan motion
 - Acquisition of the Sun was always successful after implementation of the above modifications.
 - Sun tracking
 - ASM < 0.02° within requirement
 - ESM < 0.012° within requirement
- Note: the distortion of the Sun image in elevation direction at low altitude due to refraction cannot be accounted for by the SFS and the control system.
- Sun diffuser state execution was performed successfully for the ESM and the ASM diffuser.
 - Model assumptions used for Sun occultation states and sub-solar states, calculation of the target parameters for the defined sun fixed event by the MPS-CFI, definition of the state and timing within the timeline proofed to be correct and suitable for the capabilities of SFS.

5.5.2 Moon target

Contrary to Sun states nearly every execution of a moon state in the lower atmosphere caused error messages since the moon target was not detected or lost. This was partly expected as the moon is mostly observed, when the atmosphere is illuminated by the sun. Since the SFS has a FoV of 2,1°x 2,1° the relation of the total FoV of the SFS to the moon area is about 22. In sun lit conditions and in particular with some cloud coverage in the lower part of the SFS-FoV the moon cannot be discriminated from the 'bright' background. Thus the 'normal' atmosphere prevents the SFS from successful operation.

- Acquisition of the moon was successful for calibration measurements observations above the atmosphere.
- Moon tracking in 'dark' atmosphere conditions and 'above' atmosphere
 - ASM < 0.02° within requirement
 - ESM < 0.02° within requirement

5.6 Conclusions

The current evaluation status of the 'SFS'-measurements indicates, that only minor modifications are needed to upgrade the present parameter status to the 'Final' flight status.

For Sun oriented measurements the modifications are close to finalisation and will be tested in the coming Δ -SODAP window of SCIAMACHY. The likely effect of the atmospheric refraction on the acquisition in azimuth is under investigation, but considered to be minor for the pointing performance at Sun measurements.

For moon oriented measurements states starting the measurement program above the atmosphere can remain unaltered. For all states to be executed in the occultation window plans are under consideration to modify the scenario used and as well to modify the state implementation to become independent from the SFS.

6 Pointing Performance and Geolocation

6.1 Limb Tangent Height Verification

SCIAMACHY is performing limb scattering measurements of Earth's atmosphere [2]. Atmospheric parameter profiles are retrieved from these. Knowledge of the vertical pointing during the limb measurements can be the dominating source of errors for the retrievals. In limb viewing mode, the instrument scans the scattered atmospheric limb radiance. One scan sequence consists of 35 horizontal (azimuth) scans, each with a different tangent height. The difference between two adjacent tangent heights, the so-called tangent height step size, can be commanded from ground and 3.3 km are selected as the current baseline. The height of the instantaneous field of view (IFOV) at the tangent point is 2.8 km. Special measurements with a tangent height step of 1.7 km were executed on 26th May 2002 (orbit 1230) dedicated to verify the SCIAMACHY's vertical pointing performance and resolution for the limb geometry.

The engineering pointing information which is delivered by ESA in the SCIAMACHY products is calculated from the satellite's location and orientation (measured with star sensors on board ENVISAT) and SCIAMACHY's internal scan mirror positions. The expected errors of the engineering pointing information ("pointing knowledge error") has been derived from on-ground verification of SCIAMACHY and Envisat performance [19]:

- The absolute pointing knowledge error is the deviation between the actual and the engineering instrument line of sight (ILOS): 0.079 deg (4.6 km).
- The cycle step height (knowledge) error is the maximum deviation between the actual average observation step height and the desired average observation step height between any two steps of one (vertical) scan cycle: 0.019 deg (1 km).
- The relative pointing (knowledge) error is the deviation between the actual observation height of the ILOS during one azimuth scan and the average observation height during the scan: 0.027 deg (1.6 km).

During the commissioning phase, the pointing information for target tracking observation modes (solar and lunar occultation) was directly tested by commanding the instrument to point where the sun and moon theoretically should be. A comparison with sun/moon follower data revealed that the actual ILOS was consistent with the desired one within the equivalent of less than 0.5 km tangent height variation. This improvement over the expected absolute pointing error is mainly attributed to the very good accuracy of Envisat's star trackers. In this section the verification of the pointing performance w.r.t. the accurate determination of the tangent height in limb is described. The basic idea is to use the well known height dependence of the solar backscatter signal in the upper stratosphere to verify the tangent height determination. In [20] the so called "knee" method for 335 nm wavelength is suggested: It is based on the fact that the UV radiance for tangent points in the upper stratosphere depends mainly on two parameters which have a small variance and which are known from climatologies with good accuracy above 40 km, i.e. O₃ and number density (pressure). The term "knee" refers to the fact that the radiance is maximal for a characteristic tangent height and clearly decreases for those below and above. In [21] the method is extended to 305 nm to detect a systematic offset error in the engineering tangent height information of the space-borne spectrometer OSIRIS [22]. The UV-knee method was also applied to SCIAMACHY data and a tangent height accuracy of better than 200 m was reported [23]. Nevertheless systematic errors of the order of 1 km for the tangent height offset retrieval from an individual retrieval are introduced by the pressure and O₃ uncertainties [21].

To overcome this deficiency an improved algorithm based on the original idea of Janz et al. was developed and applied to SCIAMACHY data [24]. It is distinct from the methods mentioned above since it uses neither a priori information nor the hydrostatic equilibrium assumption. The algorithm is a generalisation of the knee method as it is based on the special behaviour of the limb radiances in the UV-B spectral region. The independence of a priori information is achieved by rigorously exploiting the behaviour in a sufficiently large fit window in the UV. The algorithm determines the tangent heights by fitting a radiative transfer model to all spectral points in a UV-B fit window. The fit is performed for the whole tangent height sequence simultaneously. Inversion of tangent height, pressure and O₃ profile is based on an iterative optimal estimation algorithm [25]. Details about the algorithm and its application can be found in [24]. From sensitivity studies performed it can be concluded that the single scattering approximation can be used safely if the upper boundary wavelength is not higher than about 310 nm. With 310 nm upper boundary, the theoretical retrieval precision for tangent heights in the 33–54 km range reaches 100 m.

SCIAMACHY's limb measurements with 1.6 km tangent height step size (orbit 1230) yield particularly precise pointing information as they exhibit a relatively large number of different tangent heights in the upper stratosphere. Upon application of the TRUE algorithm to the measurement the following parameters are retrieved:

	Engineering	retrieved value	retrieval std. dev
mean tangent height [km]	45.469	45.892	0.083
tangent height step [km]	1.638	1.700	0.016
quadratic term [km]	N/A	0.0001	0.002

Table 3: Results of tangent height retrieval from SCIAMACHY limb backscatter measurements in the UV.

A new algorithm for tangent height retrieval from limb UV-B scattering measurements of the upper stratosphere was developed, tested and applied successfully to SCIAMACHY limb backscatter data. The algorithm does not rely on any a priori information on the atmospheric state nor on any approximation like the barometric formula. The application of the TRUE algorithm to a limb measurement by SCIAMACHY yields the tangent heights between 33 and 54 km with a theoretical precision of about 100 m. The methods demonstrates that the engineering pointing information is within 200 –100 km, in line with the findings in [23] and factors better than expected from on-ground tests of SCIAMACHY and ENVISAT [19]. The orbital dependence of limb the tangent height determination will be studied more systematically in the near future. It has to be noted that within the tangent height verification for solar occultation measurements a systematic off set in elevation of approx. 2 km is observed, which is currently under investigation [9].

6.2 Geolocation in Data Products

The analysis is based on scanner readouts and orbital parameters taken from selected SCIAMACHY Level 0 data for several observational modes (nadir, limb, solar occultation, sun fast sweep, subsolar). From these data the geolocation is computed using the ESA CFI s/w. ENVISAT attitude information and SCIAMACHY misalignment values are taken into account. The results are compared with expected values (from the DMOP, i.e. the SOST web page) and corner coordinates from the corresponding Level 1b product.

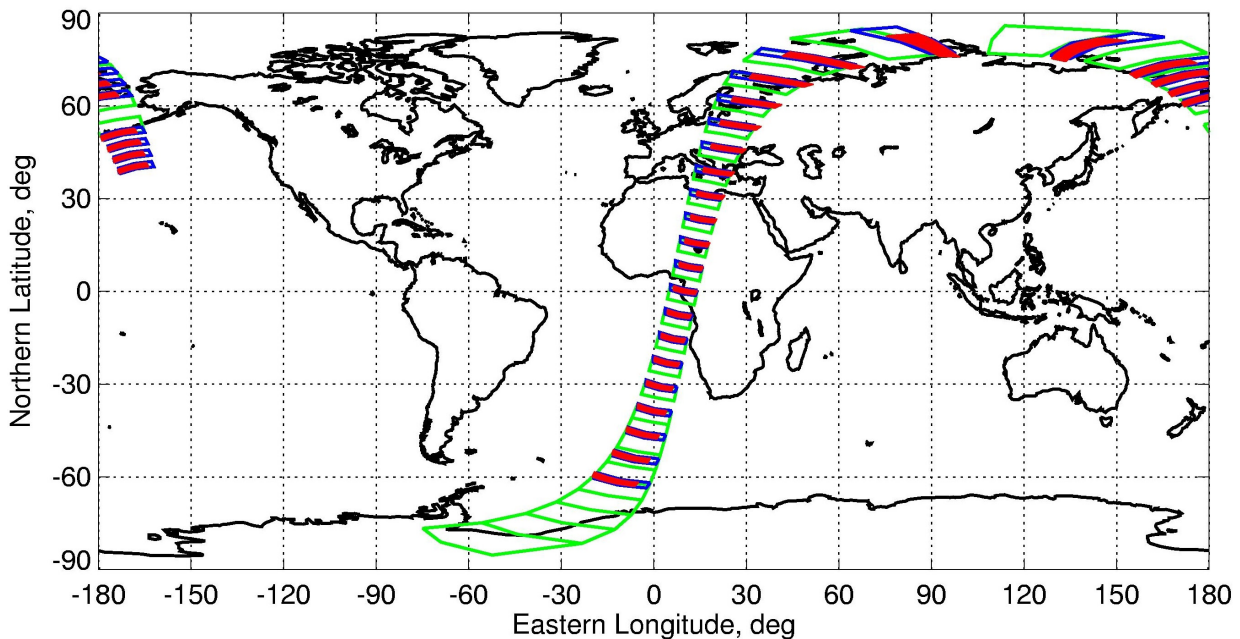


Fig. 15: Ground pixels of nadir and limb measurements in orbit 1779. Green = Expected nadir ground pixels, Blue = Expected limb ground pixels, Red = Limb Level 0 scanner data.

The results show that the geolocation derived from level 0 data is in line with level 1. Furthermore there is a good agreement between the expected and the actual geolocation for nadir. However, there seems to be systematic deviation for limb. Limb ground pixels are shifted to the left (w.r.t. flight direction) on the northern hemisphere, and to the right on the southern hemisphere. Around the equator the agreement is quite good. As a consequence, limb-nadir matching

across track is only partly achieved, although there is a good match for the prediction (see Fig. 15). Similar azimuthal effects are seen in other measurement modes (solar occultation, sun fast sweep, subsolar), although it is currently unclear if they have the same reason. An anomaly report has been issued; the problem is under discussion but not solved yet.

7 Instrument States

SCIAMACHY measurements are implemented via states and timelines. A state is a combination of instrument parameters (like exposure times, coadding factors, scanner parameters, ...). 70 states are stored on-board; they may be updated from the ground. Timelines are predefined sequences of states, which are commanded via mission planning. There are different states for different measurement types (nadir, limb, solar/lunar occultation, calibration/monitoring). Especially, there have been defined several states for nadir and limb measurements at different orbital positions in order to optimise instrument operations and thus data product quality. The settings of nadir and limb states are generally trade-off between spatial resolution, signal-to-noise, and data rate limitations.

A “best effort” set of states is used for the first validation activities. These so-called “consolidated beta states” are based on simulations and first commissioning phase results. The settings of these states are expected to be very close to final ones. The consolidated beta states are active since 18 July 2002. Final flight states will probably be defined by the end of 2002. For the analysis described here all measurements between 18 July and 1 September 2002, for which Level 0 data were available, have been taken into account. However, this paper concentrates on scientific measurements (nadir measurements, limb measurements, and solar/lunar occultation measurements). Main focus is placed on performance aspects, i.e. do the states perform as expected, and especially does saturation occur.

It shall be remarked here that channel 7 and 8 data have not been analysed in detail because of the throughput/ice problem and a missing actual dead/bad pixel mask. Moreover, it has been decided to accept spurious saturation in channel 5 for limb states at low (tropospheric) tangent altitudes in favour of a high horizontal spatial resolution. The reader should furthermore keep in mind that saturation is typically restricted to certain channels/pixel regions (mainly in the visible part of the spectrum). Also, not all readouts are affected by saturation, so even a “saturated” state typically contains a lot of useful data. Since final results on saturation of states require the analysis of non-coadded data all results described here have to be re-checked after the execution of special high data rate orbits, which is planned for end of September 2002.

During the time interval of the analysis eight different **nadir** states (seven on the dayside and one eclipse state) have been run. In total, 10255 nadir states have been analysed of which only 40 showed saturation. In four cases this saturation could be explained by sun glint (which is no problem as this should be flagged in the level 1b data product). In 24 cases the saturation could be attributed to wrong timing, i.e. the states have been executed at a wrong orbital position. This occurred typically after lunar occultation measurements on the southern hemisphere and will be corrected by updated timelines. In 14 cases there occurred saturation for no specific reason; the incoming light intensity was just a factor of up to 50% too high for a few (<5) readouts. This problem occurred typically at higher latitudes and will be covered at least partly by the above mentioned timeline update. A final decision on further modifications to prevent saturation in these cases is currently outstanding. All in all, the analysis has shown that 99.6% nadir states behave correctly.

For **limb** the situation is even better. Six different limb states have been run on the dayside, and only 9 of a total of 7757 limb states show unexpected saturation, i.e. 99.9% of the limb states are working fine. Seven times saturation occurred at tangent altitudes close to surface, which is not surprising as the limb state settings have been optimised for the stratosphere. It is suggested not to reduce the respective exposure time settings to keep the spatial resolution. In two cases the timing of one limb state was wrong after a subsolar measurement. This will be corrected by a timeline update.

Solar occultation measurement are usually performed once per orbit during sunrise over the northern hemisphere. There are two (scientific) solar occultation states. In both states the instrument scans over sun while following sunrise, but the duration of the states is different. Additionally, a state in which scanning over the sun is replaced by pointing to sun centre has been defined, but this state was not run in the time interval of the analysis. Moreover, several solar calibration states are executed at high tangent altitudes. In all cases, there was no saturation for solar observations, the scans are correct, so all solar occultation states are in good shape.

Lunar occultation measurements are possible for about one week per month during moonrise over the southern hemisphere. Because of the sun-fixed Envisat orbit, moon measurements are highly variable in time and location along the orbit, which results in a rather complex mission planning. Lunar occultation states start at about 17 km tangent altitude and follow the moonrise while pointing to the lunar centre. Additionally, there is special state for tropospheric lunar occultation, which has not been tested yet, and several lunar calibration states which are executed at high tangent altitudes. During commissioning it was verified that lunar occultation on the night side can be performed as expected, but it was identified that lunar occultation measurements in the illuminated part of the atmosphere revealed a general problem. For lunar occultation measurements on the dayside the lunar centre is lost or not even detected because of the bright limb background in the large sun follower field of view. This is a principal problem of atmospheric physics and thus can not be solved by a re-definition of state parameters. As a consequence, lunar occultation currently only works when the tangent point is on the night side. Currently, there are several solutions under discussion. A currently preferred solution is to change the mission scenario such that in case the lunar occultation tangent points are on the day side other measurements (most likely nadir) are performed instead.

It can be concluded that although it is only a “best effort” set the performance of the “consolidated beta states” is very close to nominal. More than 99% of nadir and limb measurements and all solar occultation measurements work as expected. Only lunar occultation measurements currently only work when the tangent point is on the night side. This is an open issue which has to be solved before the definition of final flight states end of this year. The main outstanding activity for definition of final flight states will be the execution and analysis of the special high data rate orbits.

8 Summary and Conclusions

After 6 month in orbit ...

- The in-flight spectral calibration differs only in the range of $\pm 0.05\text{nm}$ from the on-ground calibration for channels 1 to 6. The orbit stability of the spectral calibration is very high (close or less a 1/100 pixel). The SLS line positions are also very stable over month as the in-flight spectral calibration derived from SLS spectra from orbits 906 to 2500 vary only within $\pm 0.02\text{nm}$. A tangent height dependent spectral shift in the limb measurements is identified and its origin is clarified.
- The overall changes in the instrument throughput between on ground and in-flight are at least within 2.5% until April 2002. After that a degradation in the UV throughput of the same order of magnitude as in GOME-1 was observed and the water ice on channels 7 and 8 influences the NIR throughput. The latter can be completely removed by heating up parts of the instrument. The degradation in the UV will be monitored and further investigated and will be accounted for in 0-1 processing by the m-factor concept.
- W.r.t. to changing detector etalon the remaining weak etalon structure in SCIAMACHY was stable during the first month of commissioning. There seems to be no hints for a changing ice layer on detectors channel 1-6.
- The detector systems behaves very well. Leakage current and its temperature dependence is well characterised and in some channels even lower then determined on ground. Channel 6-8 dark signal is dominated by the thermal background and needs some further investigations to determine the correct orbit dependence to be used in the 0-1 processor.
- From the results on instrument throughput and in-flight detector characterisation in can be concluded preliminary that the demanding signal-to-noise requirements will be met in-flight.
- The monitoring of the long term behaviour of the optical system (“calibration maintenance”) has started and is currently limited by the non-availability of a sound consolidated level 1 product.
- The performance of the sun follower system is well within specification.
- The limb pointing performance is factors better than expected from the conservative estimates from the SCIAMACHY and ENVISAT on ground tests. Tangent height accuracies of 100 –200 m are achievable.
- The on-board tables defining the measurement parameters (integration time, scan profile etc.) were fine tuned with the result that since end of July SCIAMACHY is continuously and successfully performing its nominal measurement program and over 99.5 % of all scientific measurements are working as expected.

From this all it can be concluded that from instrument performance and calibration point of view SCIAMACHY is ready for validation since August 2002.

9 Acknowledgements

The authors would like to thank Ch. Chlebek and the team at DLR Bonn as well as R. van Konijnenburg and the team at NIVR for all their efforts spent over more than ten years on managing the SCIAMACHY project. Also the support of ESA during commissioning phase and its preparation, and especially the support by the teams at ESOC and ESTEC is kindly acknowledged.

10 References

1. Burrows et al., SCIAMACHY - A European proposal for atmospheric remote sensing from the ESA Polar Platform, published by Max-Planck-Institut für Chemie, 55122 Mainz, Germany, 1988
2. H. Bovensmann, J. P. Burrows, M. Buchwitz, J. Frerick, S. Noel, V.V. Rozanov, K.V.Chance, A.P.H.Goede. SCIAMACHY: Mission objectives and measurement modes, *Journal of the Atmospheric Sciences*, 56, 127–150, 1999
3. SCIAMACHY Performance Summary Report, RP-SCIA-0000FO/117, 2001
4. OPTEC5: Wavelength calibration of the SCIAMACHY PFM, RP-SCIA-1000TP/266, issue 1, 4 December 2000.
5. New spectral calibration of SCIAMACHY channels 7 and 8 using gas cell absorption spectra, SRON-EOS-HS-0001, issue 1, 3 February 2000
6. Wavelength and slitfunction calibration of the SCIAMACHY PFM, TN-SCI-1000TP/189, February 1999
7. Sioris, C. E., et al., Stratospheric profiles of nitrogen dioxide observed by OSIRIS on the Odin satellite, submitted to *JGR*, 2002.
8. Christian von Savigny, Alexei Rozanov, Huib Visser Semi-quantitative estimate of spectral shifts in SCIAMACHY limb observations, University of Bremen, 2002
9. A. Schlesier, J. Meyer, L. K. Amekudzi; SCIAMACHY occultation calibration, IUP Bremen, 2002
10. Maurilies et al., First results on NIR retrieval at SRON, priv. com., 2002
11. M. Buchwitz et al., SCIAMACHY on ENVISAT: Trace Gas Vertical Column Retrieval using Channel 8 Nadir Measurements: First Preliminary Results, Proc. ENVISAT Calibration Review, SP-520, 2002
12. ENV-ATB-DLR-SCIA-0041
13. SCIAMACHY SODAP: Memory effect at state initialisation, SRON-SCIA-PHE-RP-005
14. TR-SCIA-1120SR/37-44
15. SCIAMACHY SODAP Objective 38: Leakage current versus temperature, SRON-SCIA-PHE-RP-006
16. SCIAMACHY Operational Long-Term Monitoring, PO-TN-DLR-SH-0004
17. GOME Data Quality Improvement Final Report, TN-GDAQI-003SR/2000
18. Gottwald et al. SCIAMACHY operations support overview, Proc. ENVISAT Calibration Review, SP-520, 2002
19. A. Schwab, SCIAMACHY Pointing error budget, Technical Report TN-SCIA-0000DO/06, Feb 1999. issue D
20. Scott J. Janz, Ernest Hilsenrath, Dave Flittner, and Donal Heath. Rayleigh scattering attitude sensor. Proc. SPIE, 2831(45):146–153, 1996.
21. C. E. Sioris, C. von Savigny, R. L. Gattinger, J. C. McConnell, I. C. McDade, E. Griffioen, and E. J. Llewellyn. Attitude determination for limb-scanning satellites: The "knee" at 305 nm. In Fall Meet. Suppl., Eos Trans. AGU, 2001. Abstract A32B-0056.
22. E.J. Llewellyn, D.A. Degenstein, I.C. McDade, R.L. Gattinger, R. King, R. Buckingham, E.H. Richardson, D.P. Murtagh, W.F.J. Evans, B.H. Solheim, K. Strong, and J.C. Mc-Connell. OSIRIS: An application of tomography for absorbed emissions in remote sensing. In G.A. Lampropoulos and R.A. Lessard, editors, *Applications of Photonic Technology*, volume 2, pages 627–632. Plenum, New York, 1997
23. Sioris et al. Tangent height verification algorithm, SCIAVALIG Web, July 2002
24. Kaiser et al., SCIAMACHY Limb Scattering: Pointing Knowledge and Retrieval in the UV-B, University of Bremen, Germany, 2002
25. C.D. Rodgers. Retrieval of atmospheric temperature and composition from remote measurements of thermal radiation. *Reviews of Geophysics and Space Physics*, 14(4):609–624, 1976.